Evaluation of *Kleinhovia hospita* Metabolite Profiles Exposed to Diverse Gamma-Irradiation Doses by ^{1}H-NMR Combined with Chemometric Modeling

Islamudin Ahmad[1,2], Lizma Febrina[1,2*], Herman Herman[1,2], Baso Didik Hikmawan[1,2], Amal Rezka Putra[3], Junaidin Junaidin[1,2], Arman Rusman[1,2], Arsyik Ibrahim[1,2], Hifdzur Rashif Rija'i[1,2], Erwin Samsul[1,2], Muhammad Arifuddin[1,2], Supriatno Salam[1,2], Iswahyudi Iswahyudi[2], Gemini Alam[4], and Abdul Mun'in[5]

[1]*Pharmaceutical Research and Development Laboratory of FARMAKA TROPIS, Faculty of Pharmacy, Universitas Mulawarman, Kampus Gunung Kelua, Samarinda 75119, Indonesia*

[2]*Department of Research and Development, PT. Borneo Riseta Naturafarm, Jl. Simpur No. 47, Tenggarong Sebrang, Kutai Kertanegara 75572, Indonesia*

[3]*Research Center for Radioisotope, Radiopharmaceutical, and Biodosimetry Technology, Research Organization for Nuclear Energy, National Research and Innovation Agency (BRIN), Kawasan Puspiptek, Building 720, Serpong, Banten 15314, Indonesia*

[4]*Department of Pharmacognosy, Faculty of Pharmacy, Hasanuddin University, Jl. Perintis Kemerdekaan Km. 10, Kampus UNHAS Tamalanrea, Makassar 90245, Indonesia*

[5]*Department of Pharmacognosy-Phytochemistry, Faculty of Pharmacy, Universitas Indonesia, Jl. Kukusan Beji, Depok 16424, Indonesia*

* ***Corresponding author:***

email: lizma@farmasi.unmul.ac.id

Received: January 7, 2025
Accepted: December 24, 2025

DOI: 10.22146/ijc.103509

Abstract: *Gamma irradiation is a widely used method for decontaminating medicinal plants, including* Kleinhovia hospita *(Tahongai). However, the high energy inherent in this process, coupled with the paucity of scientific reports detailing changes in the* K. hospita *metabolite profile, necessitates an investigation into its effects. Hence, this study examined the effects of gamma irradiation at varying doses (0–25 kGy) on the metabolite profile of the ethanolic extract of* K. hospita *utilizing ^{1}H-NMR combined with a chemometric approach. The concentrations of some identified metabolites present in the sample were determined by the quantitative ^{1}H-NMR technique. Our investigation successfully identified 20 metabolites in the* K. hospita *sample. Both the quantitative analysis and the PLS-DA modeling demonstrated that gamma irradiation doses up to 5 kGy induced no significant differences in the metabolite profiles (p-value > 0.05), indicating high similarity with the control group. Conversely, a significant alteration in the metabolite profile emerged only at an exposure dose of 10 kGy or higher, characterized by the loss of characteristic amino acid and cycloartane triterpenoid signals. Consequently, the 10 kGy level signifies the point at which substantial alterations to the* K. hospita *metabolome are initiated, thereby demanding prudence in its application.*

Keywords: *^{1}H-NMR; metabolomic; Tahongai; gamma-irradiation; PLSDA*

■ INTRODUCTION

The demand for natural products that are free from microbial contamination is growing worldwide. One of them is *Kleinhovia hospita* Linn, also known as Tahongai. *K. hospita* is a medicinal plant that has been reported to possess a variety of biological activities, including anti-photoaging [1], antibacterial [2], antiplasmodial and anti-Toxoplasma properties [3]. The chemical compounds present in the substance are responsible for these biological activities, including cycloartane triterpenoids, flavonoids such as quercetin, alkaloids, tannins, and steroids [4-5]. This property permits the *K.*

hospita plant to be utilized extensively by the public in the preparation of decoctions, tea, and a variety of pharmaceutical products [6]. Due to the growing popularity of *K. hospita*, it is crucial to ensure the safety and purity of the product for the public, particularly by safeguarding it from the risks of contamination.

Contamination, which may include fungus and microbial contamination, is one of the most significant concerns regarding the safety of herbal medicines [7]. This contamination may be present in all parts of herbal medicines, such as seeds, roots, stems, leaves, and flowers. This contaminant may manifest itself during the cultivation process or subsequent postharvest operations. The likelihood of contamination during the growth process will be elevated in regions with high humidity and rainfall. Apart from that, the quality of this *K. hospita* product is also significantly influenced by storage conditions. This issue is more prevalent in tropical and subtropical regions, as high temperatures and water levels promote the production of toxins and fungal growth [8-9]. To satisfy the requirement and obtain a safer and more effective herbal medicine, numerous efforts have been undertaken to remove contaminants and safeguard these plants for medicinal use. Decontamination has been attempted through various methods, including thermal treatment, ultraviolet radiation, fumigation, and gamma irradiation (GI) [10-11]. Nevertheless, thermal treatment is frequently unfeasible because of the volatility and sensitivity of chemical compounds in medicinal plants, whereas UV irradiation is rarely effective due to its limited energy input.

Since 2017, the use of GI for preserving medicinal plants has been on the rise, as it can effectively reduce microbial contamination [12-14]. GI is the process of sterilizing or decontaminating materials through destroying the genetic material of microorganisms using gamma rays, which are ionizing radiation typically derived from cobalt [12]. The mechanism involves the penetration of high-energy photons (γ-rays), which induce ionization and the subsequent formation of highly reactive free radicals, such as the hydroxyl radical (•OH), generated from water radiolysis. While this process is fundamental to pathogen inactivation, the same powerful reactivity, particularly at high doses, also causes the undesirable degradation of plant metabolites, as free radicals attack both microbial and host plant cellular components [15-17]. However, the extent of the effect produced by GI is contingent upon various factors, such as the resistance of cells to radiation [18-20]. Therefore, it is imperative to meticulously evaluate the irradiation dose range to prevent the degradation of active metabolites in *K. hospita*, as such degradation could influence its inherent pharmacological activity.

Currently, research on the application of varying dosages of GI to *K. hospita* remains quite limited, particularly regarding its effects on the metabolite profile. This study presents the inaugural scientific report examining the impact of GI on the metabolite profile of an ethanol extract using ^{1}H-NMR-based metabolomics. This approach has been effectively applied to investigate the metabolomes of extracts containing intricate metabolites, such as those from *Eleutherine bulbosa*, rice, and civet coffee [21-23]. The utilization of NMR for metabolite analysis offers numerous benefits, including effortless sample preparation, nondestructive samples, a more comprehensive metabolite profile (not exclusively reliant on volatile metabolites), and the ability to quantify them. To the best of our knowledge, the application of NMR-based metabolomics to the of *K. hospita* has not been previously reported.

■ EXPERIMENTAL SECTION

Materials

The *K. hospita* leaves utilized in the present research were gathered from the village of Tuana Tuha, Kenohan District, Kutai Kartanegara Regency. The samples were subsequently analyzed at the Dendrology Laboratory within the Faculty of Forestry at Mulawarman University (003/BRN/2024). Concurrently, ethanol was employed as an extraction solvent.

Instrumentation

The following instruments were used for sample processing and analysis: a mechanical grinder (4100W, Wangshuiyan, China), a Co-60 Merah Putih GI (BRIN

PUSPIPTEK, Serpong, Indonesia), an R-210 Series rotary evaporator (Buchi, Switzerland), an MC-12 microcentrifuge (Benchmark Scientific, USA), and an Inova 500 MHz NMR spectrometer (Agilent Technologies, USA).

Procedure

Preparation of samples and gamma irradiation

The collected *K. hospita* samples were first subjected to wet sorting to remove all extraneous matter and undesired vegetative material. Following this, the samples were thoroughly washed with running water. Then, the *K. hospita* samples were dried on net racks in a well-ventilated room at a temperature below 40 °C for 7 d. Dried *K. hospita* leaf samples were ground into powder using a mechanical grinder. The irradiation of *K. hospita* was conducted at the IGMP facility in South Tangerang, Indonesia, with a maximum capacity of 2 MCi, utilizing a Co-60 radioactive source. The source is stored in a demineralized water pond measuring $3.6 \times 2.8 \times 6.0$ m^3, serving as both a cooler and a radiation shield. During operation, the radioactive source is elevated above the pool to facilitate radiation exposure to the sample. The pool is situated within an irradiation chamber bunker, shielded by over 1.8 m of concrete, with a labyrinthine access for goods and regulated pathways for maintenance activities. The extract is prepared in an appropriate container, such as plastic, labeled according to the intended dosage, and stored in a designated carrier. Irradiation was performed with incremental doses of 1, 5, 10, 15, 20, and 25 kGy, with exposure time determined by the specified dose level. Untreated samples were used as control groups. Biological replication was performed 6 times per test group. Upon completion, the sample is extracted and preserved for subsequent analysis [24].

Extraction and preparation of K. hospita *for NMR analyzation*

Utilizing 96% ethanol as a solvent, the maceration method was employed to extract 150.0 g of desiccated *K. hospita* powder. The extraction process was carried out throughout the course of 24 h to complete. Whatman filter paper was employed to isolate the residue from the filtrate. The residual was macerated three more times. The filtrate was collected and dried using a rotary evaporator at approximately 50 °C to generate a viscous extract. Next, 800 mg of the *K. hospita* ethanol extract was combined with 1 mL of pH 7.0 phosphate-buffered methanol-deuterium (CD_3OD containing phosphate buffer) that had been supplemented with 1.0 mM TSP or 3-(trimethylsilyl)-2,2,3,3-tetradeuteropropionic acid sodium salt. The mixture was homogenized for 1 min and subsequently centrifuged in an MC-12 microcentrifuge at 12,000 rpm for 5 min. Approximately 600 µL of the filtrate fluid was transferred to an NMR tube for analysis.

Analyzing using NMR spectroscopy

NMR measurements were conducted on each *K. hospita* sample. The NMR was utilized to record the ^{1}H-NMR spectra. The measurement was carried out with the help of pre-saturation software, with an acquisition time of 2.72 s, a delay time of 2.00 s, 64,000 data points, a spectral width of 8,012 Hz, and 128 total scans. For further processing, the NMR FID data were imported into the ACD/Labs12.0 program. Two-dimensional NMR experiments, which used 4 scans with increments of 512 for COSY analysis, 256 for TOCSY analysis, and 128 for J-resolved analysis, respectively, further validated the distinctive signals of the identified metabolites in the ^{1}H-NMR spectra. The ^{13}C-NMR spectra were acquired using the following parameters: 64,000 data points, a spectral width of 31,422 Hz, an acquisition duration of 1.04 s, a delay time of 2.0 s, and 10,000 scans were performed. The ^{1}H–^{13}C HSQC spectrum of the sample was performed in phase-sensitive mode. The acquisition parameters were specified as follows: The dataset comprises 833 points of data for ^{1}H and 256 points of data for ^{13}C-NMR. The spectral widths are 5.195 Hz for ^{1}H and 25.141 Hz for ^{13}C. The acquisition duration is 0.160 s, the delay duration is 1.5 s, and 8 dummy scans are conducted, for a total of 16 scans. In the absolute mode, the ^{1}H–^{13}C HMBC spectrum was obtained using the specified parameters. In contrast, the F1 (^{13}C) dataset comprises 768 data points, whereas the F2 (^{1}H) dataset comprises 1490. In F2 (^{1}H), the spectral width is 5751.3 Hz, whereas in F1 (^{13}C), it is 30165.9 Hz. There are 40 scans

in total, with an acquisition time of 0.259 s and a delay time of 2.0 s. Additionally, there are 4 dummy scans [23].

Relative quantification ^{1}H-NMR analysis

Quantification of metabolites in the samples was performed according to the protocol described by Gao et al. [25]. The concentration of each metabolite was determined ratiometrically by comparing the integral of its characteristic signal to the integral of TSP (1 mM), which served as the internal standard. The suitability of TSP as an internal standard was based on its distinct singlet peak, which assured no spectral overlap with other signals. Metabolite concentrations are reported as the mean ± standard deviation obtained from 6 biological replicates. Statistical comparisons between experimental groups were performed using a one-way analysis of variance (ANOVA), followed by post hoc analysis with Duncan's multiple-range test (all calculations were conducted in Microsoft Excel, Microsoft Office 365). Statistical significance was defined as a *p*-value less than 0.05. The concentration of each metabolite has been calculated using Eq. (1);

$$X = \frac{\text{Area}_X}{\text{Area}_{IS}} \times \frac{\text{nuclei} \in IS}{\text{nuclei} \in X} \times \text{Conc.}_{IS} \quad (1)$$

The final quantity of the metabolite of interest (X) is expressed in mM, contingent upon the unit of mass or amount utilized for the Internal Standard (IS). The integration of the spectral areas is performed using NMR software. The number of nuclei comprising the IS signal is defined by its structure, while the number of nuclei for the target metabolite is determined by the metabolite′s structure and formula, and the specific number of protons contributing to the signal at the designated chemical shift.

Processing spectral data

Spectral data were analyzed utilizing the ACD/Labs 12.0 software. According to the protocols established in previous investigations, alignment and binning of all ^{1}H-NMR spectra were performed at 0.04 ppm intervals. Data from the bucket of TSP in the 0.00 and 3.43–3.66 ppm areas, which are associated with the solvent signal, are initially excluded. Following this, the data for the area under the curve for each bucket is normalized to the total number of buckets in each spectrum. Additionally, all data were transformed using Pareto scaling prior to being subjected to multivariate statistical analysis. A series of ^{1}H-NMR data is subsequently analyzed using multivariate statistics with SIMCA Ver. 15.0 software. In this investigation, unsupervised (PCA) and supervised (PLSDA) analyses were implemented. PCA was initially implemented to facilitate data visualization and to confirm that there were no confounding outliers prior to the commencement of supervision classification. A score plot was employed to visualize PCA data. After that, PLSDA was implemented to identify the most pertinent variance for group separation. The integrated signal intensity derived from each discrete region (bin) of the ^{1}H-NMR spectrum is represented by variable X (predictor) in PSLDA, while the group data for various dose variations is represented by variable Y (response). A re-permutation test, conducted up to 200 cycles, was employed to internally validate the resultant model by examining the R^2Y value, which indicates the model's accuracy, and the Q^2 value, which indicates the accuracy of the predictions. In this work, the outcomes of PLSDA modelling were represented using score and loading plots.

■ RESULTS AND DISCUSSION

The ^{1}H-NMR spectra of all *K. hospita* samples, comprising the groups exposed to GI at doses of 1, 5, 10, 15, 20, and 25 kGy, along with untreated control group, were illustrated in the Fig. 1. Typically, the ^{1}H-NMR spectrum of *K. hospita* ethanol extract that are divided into 4 major areas: organic acid (0.38–3.00 ppm), amino acid (0.80–4.66 ppm), carbohydrate (3.01–5.52 ppm), and aromatic substances (6.0–8.5 ppm) [26]. In Fig. 1, the ^{1}H-NMR spectral fingerprint of *K. hospita* is not appreciably altered by GI at 1 and 5 kGy, thereby establishing that these low-to-moderate treatments induce no discernible qualitative shift in the sample's metabolite composition compared to the untreated sample. Conversely, samples treated with GI at 15 kGy exhibited distinct signal patterns compared with untreated samples, particularly in the ranges 0.80–2.85, 3.15–3.75, and 6.75–7.70, which are associated with amino acids, carbohydrates, and aromatic compounds, respectively. Disparities in signal patterns indicate that the metabolite profiles of samples treated with 15 kGy and

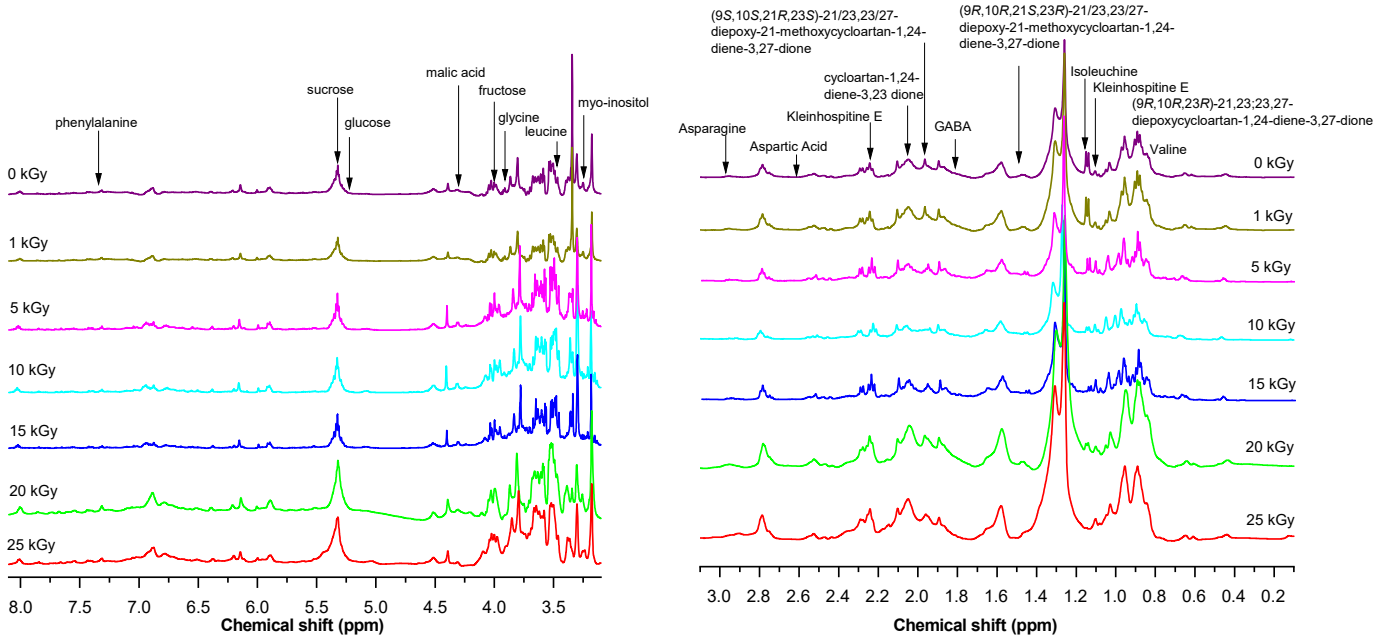

Fig 1. The ^{1}H-NMR spectra of the *K. hospita* sample

untreated samples are distinct. A signal difference was also observed in samples subjected to GI doses of 20 and 25 kGy.

Metabolite identification is implemented to comprehend the metabolites that distinguish each treatment group. Metabolites in *K. hospita* samples were identified by analyzing specific signals in the ^{1}H- and ^{13}C-NMR spectra. To validate the identification, the characteristic signals were compared with reference spectra from the metabolite database (www.hmdb.ca) and the published literature [4]. The chemical shifts of the identified metabolites may differ from those reported for the pure compounds. This results from variations in solvents, temperatures, measurement conditions, and similar factors. Consequently, this identification was reaffirmed via 2D NMR analysis of the spectral data, employing COSY, J-resolved, HSQC, and HMBC techniques (the spectra are presented in Fig. S1–S8). A total of 20 metabolites were identified in the *K. hospita*, encompassing both the treated gamma-irradiated sample and the untreated sample. These metabolites include (**1**) valine, (**2**) glycine, (**3**) isoleucine, (**4**) leucine, (**5**) asparagine, (**6**) aspartic acid, (**7**) phenylalanine, (**8**) formic acid, (**9**) malic acid, (**10**) GABA, (**11**) myo-inositol, (**12**) adenosine, (**13**) glucose, (**14**) fructose, (**15**) sucrose, (**16**) cycloartan-1,24-diene-3,23-dione, (**17**) (9*S*,10*S*,21*R*,23*S*)-21/23,23/27-diepoxy-21-methoxycycloartan-1,24-diene-3,27-dione, (**18**) (9*R*,10*R*,23*R*)-21,23;23,27-diepoxycycloartan-1,24-diene-3,27-dione, (**19**) (9*R*,10*R*,21*S*,23*R*)-21/23,23/27-diepoxy-21-methoxycycloartan-1,24-diene-3,27-dione, and (**20**) kleinhospitine E. The structures of all identified metabolites are illustrated in Fig. 2.

In all ^{1}H-NMR spectra of *K. hospita*, both treated and untreated, a doublet at 5.39 ppm was observed, a typical signal of sucrose anomeric protons. Sucrose signals were also clearly identified in the ^{1}H-NMR spectrum at 3.58, 3.79, 3.49, 3.88, 3.84, 4.23, 4.08, and 3.90 ppm. This is further evidence that sucrose is present in the *K. hospita* sample. Additional carbohydrates were also identified, including glucose and fructose. The glucose was identified by the presence of doublet signals at 5.25 and 3.56 ppm, which were correlated. According to prior research, both signals are recognized as H-1/H-2 signals from glucose [27]. Meanwhile, the H-2/H-3 correlation of fructose was discovered at 4.06/4.10 ppm. The low-intensity triplet signal observed in the sugar region, at 3.20 ppm, corresponds to myo-inositol. This compound was detected in the ^{1}H-NMR spectra of untreated *K. hospita* samples and those treated with 1 and 5 kGy. This triplet signal, associated with myo-inositol,

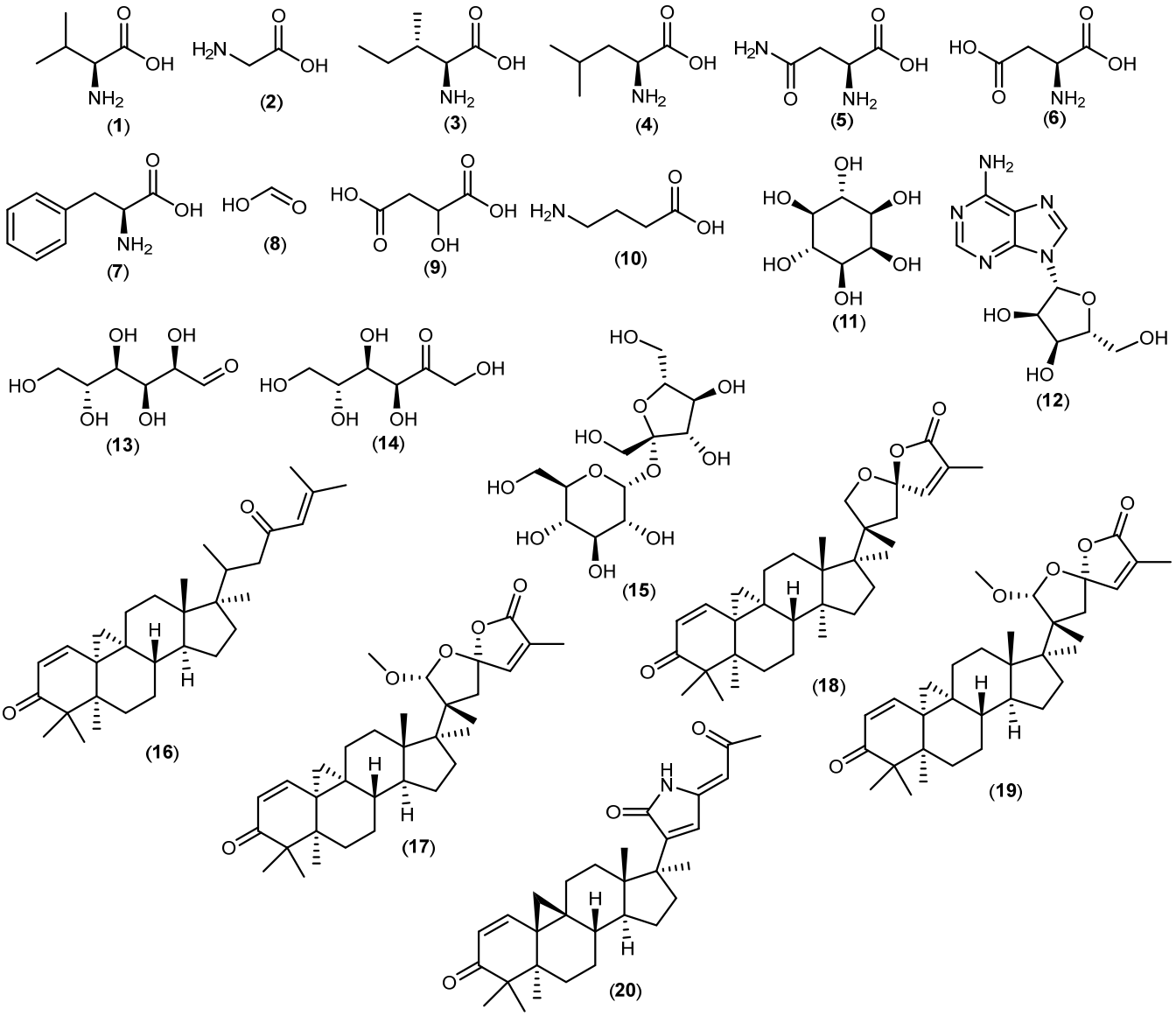

Fig 2. Identified structures in *K. hospita* ethanol extract

was not detected in the ^{1}H-NMR spectra of the 10 to 25 kGy *K. hospita* samples. Concurrently, three methylene GABA (gamma-aminobutyric acid) signals were detected in the 1.87, 2.23, and 3.01 ppm regions. Untreated samples and those treated with 1, 5, and 10 kGy could identify these three methylene signals. However, GABA signals at 20 and 25 kGy were unable to be identified.

The samples of *K. hospita* also contained malic acid, formic acid, adenosine, and (9*R*,10*R*,23*R*)-21,23;23,27-diepoxycycloartan-1,24-diene-3,27-dione, (9*S*,10*S*,21*R*,23*S*)-21/23,23/27-diepoxy-21-methoxycycloartan-1,24-diene-3,27-dione, (9*R*,10*R*,21*S*,23*R*)-21/23,23/27-diepoxy-21-methoxycycloartan-1,24-diene-3,27-dione, and kleinhospitine E. Malic acid, an organic acid, is naturally produced in the leaves of *K. hospita*. The synthesis of this compound necessitates the use of carbohydrates and phosphoenolpyruvate, which are subsequently deposited in leaf vacuoles. The compound was identified by the presence of a doublet of doublets at 2.36 and 2.65 ppm, confirming the signal of a methylene group [28]. The methine proton of malic acid was observed at 4.28 ppm. The singlet at 8.41 ppm was assigned to a proton signal from formic acid. The adenosine proton

signal (H-2, 8.21 ppm) was consistently detected in all *K. hospita* samples.

Furthermore, numerous triterpenoids were identified in *K. hospita* samples. Two AB doublet signals are observed at 0.79 and 1.38 ppm, likely corresponding to cyclopropyl protons. Additionally, 6 singlet signals are present in the methyl group regions at 0.88, 0.95, 1.06, 1.07, 1.88, and 2.15 ppm, along with three olefinic protons at 6.37, 5.89, and 6.06 ppm. The ^{13}C-NMR spectrum of *K. hospita* shows olefinic carbon signals in the ranges of 156.4, 155.2, 124.2, and 124.1 ppm. This confirms that the olefin belongs to this group. The spectrum HMBC shows a correlation between H-21/C17, H-21/C-20, H-21/C-22, H-22/C-20, H-22/C-21, H-22/C-23, H-24/C-23, H-24/C-26, H-24/C-27, H-26/C-24, and H-26/C-25. Analysis of ^{1}H- and ^{13}C-NMR signals, along with correlations observed in the HMBC spectrum, led to the identification of compounds bearing a cycloartan skeleton with an olefinic side chain. Literature studies on metabolites in *K. hospita*, along with various metabolite databases, identified the proton signals as those of (9*R*,10*R*)-cycloartan-1,24-diene-3,23-dione. Similarly, three triterpenoid compounds were identified in the ^{1}H-NMR spectrum of *K. hospita*.

Amino acids, including valine, phenylalanine, aspartic acid, asparagine, leucine, and isoleucine, were identified in *K. hospita* samples. Particularly in the ^{1}H-NMR spectra of both untreated and treated samples, at dosages of 1, 5, and 10 kGy, respectively. In contrast, typical signals of amino acids were not detectable at 15, 20, and 25 kGy. Two methyl signals from valine were identified as doublets at 0.83 and 0.85 ppm. At the same time, the methine H-3 valine signal was found around 1.99 ppm. A correlation was observed between the CH3 and H-3 valine groups in the COSY spectrum of *K. hospita*. The methyl signal of isoleucine was identified as a triplet at 0.68 ppm. This signal is correlated with the multiplet signal in the 1.20 ppm region. It was found that these two signals were linked by the methyl group and the methylene group of isoleucine, which had previously been recognized in another research [29]. Chiral leucine protons were discovered in the 3.38 ppm area, confirming a triplet signal. The multiplicity of this signal serves as confirmation that the chiral proton is near the methylene group (1.77 ppm). Additionally, the methyl group at 1.12 ppm is distantly correlated with this methylene group. In the more deshielding region (2.87 ppm), a doublet of doublets signal from the methylene group of asparagine was observed. In comparison, the doublet of doublet signal from the methylene group of aspartic acid was observed at 2.76 ppm. This is due to the deshielding effect of the amide group in asparagine on the methylene (H-3) group. Asparagine is one type of amino acid that possesses an aromatic side chain. The correlation between the aromatic protons of phenylalanine, which are 7.28, 7.33, and 7.40 ppm, was used to detect this compound [30]. An overview of the metabolite identification in the ^{1}H-NMR spectra of *K. hospita* is provided in Table 1.

The metabolite identification results indicate that the metabolite profiles of samples treated with GI differ from those of untreated samples. At doses above 10 kGy, the majority of amino acids and organic acids were not detected in the samples. Meanwhile, the signals 6.33, 5.96, 2.22, 3.59, 4.32, 1.82, and 2.18, which were identified as (9*R*,10*R*,23*R*)-21,23;23,27-diepoxycycloartan-1,24-diene-3,27-dione, were not detected in gamma-irradiated samples at 10 kGy or higher. This triterpenoid compound is reported to possess potent anti-HIV properties [4]. Even more intriguing, the metabolite profiles of samples subjected to GI at 1 and 5 kGy were qualitatively comparable to those of the untreated samples.

Table 1. The metabolites identified from the ^{1}H-NMR spectra of *K. hospita*

No	Metabolite	Data of NMR (ppm)	Sample in kGy [1)]						
			0	1	5	10	15	20	25
1	Valine	1.96 (H-3, *m*, 1H), 0.85 (CH_3, *d*, 3H, *J* = 10.1 Hz), 4.16 (H-2, *d*, 1H, *J* = 10.5 Hz)	+	+	+	+	nd	nd	nd
2	Glycine	3.95 (H-2, *d*, 1H), 3.89 (H-2, *d*, 1H)	+	+	+	nd	nd	nd	nd
3	Isoleucine	1.20 (H-4, *m*, 2H), 1.79 (H-3, *m*, 1H), 4.15 (H-2, *d*, 1H, *J* = 10.4 Hz)	+	+	+	nd	nd	nd	nd

No	Metabolite	Data of NMR (ppm)	Sample in kGy [1)]						
			0	1	5	10	15	20	25
4	Leucine	1.13 (CH3, *d*, 3H), 1.47 (H-4, *m*, 1H), 1.77 (H-3, *m*, 2H), 3.38 (H-2, *t*, 1H, *J* = 7.78 Hz)	+	+	+	nd	nd	nd	nd
5	Asparagine	2.96 (H-3, *dd*, 1H), 2.97 (H-3, *dd*, 1H)	+	+	+	+	nd	nd	nd
6	Aspartic acid	2.76 (H-3, *dd*, 2H)	+	+	+	+	nd	nd	nd
7	Phenylalanine	7.28 (H-2/H-6, *d*, 1H), 7.33 (H-4, *t*, 1H), 7.40 (H-3/H-5, *d*, 1H)	+	+	+	nd	nd	nd	nd
8	Formic acid	8.41 (H-1, *s*, 1H)	+	+	+	nd	nd	nd	nd
9	Malic acid	2.36 (H-2, *dd*, 1H), 2.65 (H-2, *dd*, 1H), 4.28 (H-1, *dd*, 1H, *J* = 16.15 Hz, 6.25 Hz)	+	+	+	+	+	+	+
10	GABA	1.87 (H-3, *m*, 2H), 2.23 (H-2, *m*, 2H), 3.01 (H-4, *t*, 2H, *J* = 12.05 Hz)	+	+	+	+	nd	nd	nd
11	Myo-inositol	3.20 (H-4, t, 1H, J= 9 Hz)	+	+	+	+	nd	nd	nd
12	Adenosine	8.21 (H-2, *s*, 1H)	+	+	+	+	+	+	+
13	Glucose	5.25 (H-1, *d*, 1H, *J* = 5.10 Hz), 3.56 (H-2, *dd*, 1H), 3.83 (H-6, *m*, 1H)	+	+	+	+	+	+	+
14	Fructose	4.07 (H-1, *d*, 2H, *J* = 9.5 Hz), 4.13 (H-3, *d*,1H, *J* = 9.5 Hz), 3.88 (H-5, *m*, 1H)	+	+	+	+	+	+	+
15	Sucrose	5.38 (H-1, *d*,1H, *J* = 5.10 Hz), 3.58 (H-2, *dd*, 1H, *J* = 10.60 Hz, *J* = 5.10 Hz), 3.79 (H-3, *t*, 1H, *J* = 9.51 Hz), 3.49 (H-4, *t*, 1H, *J* = 9.51 Hz), 3.88 (H-5, *dd*, 2H), 3.84 (H-6, *m*, 1H), 4.23 (H-3', *d*, 1H), 4.08 (H-4', *t*, 1H, *J* = 9.52 Hz), 3.90 (H-5', *dd*, 2H, *J* = 6.52 Hz, *J* = 3.67 Hz)	+	+	+	+	+	+	+
16	Cycloartan-1,24-diene-3,23-dione	6.37 (H-1, *d*, 1H, *J* = 10.2 Hz), 5.89 (H-2, *d*, 1H, *J* = 10.2 Hz), 2.24 (H-5, *m*, 1H), 1.27 (H-6, *m*, 2H), 1.32 (H-7, *m*, 2H), 1.97 (H-8, *m*, 1H), 1.23 (H-11, *m*, 1H), 2.08 (H-11, *m*, 1H), 1.46 (H-12, *m*, 1H), 1.22 (H-15, *m*, 1H), 1.36 (H-15, *m*, 1H), 1.32 (H-16, *m*, 1H), 1.88 (H-17, *m*, 1H), 1.58 (H-18, *m*, 3H), 1.0 (H-19, *s*), 0.79 (H-19, *d*, 3H, *J* = 5.2 Hz), 1.88 (H-26, *s*, 3H), 2.15 (H-27, *s*, 3H), 1.05 (H-28, *s*, 3H), 1.06 (H-29, *s*, 3H), 0.88 (H-30, *s*, 3H)	+	+	+	+	nd	nd	nd
17	(9*S*,10*S*,21*R*,23*S*)-21/23, 23/27-diepoxy-21-methoxycycloartan-1,24-diene-3,27-dione	6.77 (H-1, *d*, 1H, *J* = 10.1 Hz), 5.90 (H-2, *d*, 1H), 2.17 (H-5, *m*, 1H), 1.10 (H-6, *m*, 1H), 1.58 (H-6, *m*, 1H), 1.21 (H-7, *m*, 1H), 2.05 (H-8, *m*, 1H), 1.67 (H-11, *m*,1H), 1.86 (H-11, *m*, 1H), 2.17 (H-17, *m*, 1H), 1.04 (H-18, *m*, 3H), 0.71 (H-19, *d*, 1H), 1.45 (H-19, *d*, 1H), 1.09 (H-28, *s*, 3H), 0.95 (H-29, *s*, 3H), 0.89 (H-30, *s*, 3H)	+	+	+	+	nd	nd	nd
18	(9*R*,10*R*,23*R*)-21,23;23,27-diepoxycycloartan-1,24-diene-3,27-dione	6.33 (H-1, *d*, 1H, *J* = 10.1 Hz), 5.96 (H-2, *d*, 1H, *J* = 10.1 Hz), 2.22 (H-5, *t*, 1H, *J* = 8.7 Hz), 1.23 (H-6a, *m*, 1H), 1.58 (H-6, *m*, 1H), 1.38 (H-7, *m*, 2H), 2.03 (H-8, *t*, 1H), 1.68 (H-11, *m*, 1H), 1.19 (H-12, *m*, 1H), 0.94 (H-19, *s*, 3H), 0.78 (H-19, *d*, 3H, *J* = 5.01 Hz), 1.38 (H-20, *d*, 3H, *J* = 5.01 Hz), 4.32 (H-21, *t*, 1H, *J* = 8.5 Hz), 1.82 (H-22, *m*, 1H), 6.69 (H-24, *s*, 1H), 1,93 (H-26, *s*, 3H), 1.06 (H-28, *s*, 3H), 1.07 (H-29, *s*, 3H), 0.89 (H-30, *s*, 3H)	+	+	+	+	nd	nd	nd
19	(9*R*,10*R*,21*S*,23*R*)-2½3,23/27-diepoxy-21-methoxycycloartan-1,24-diene-3,27-dione	6.38 (H-1, *d*, 1H, *J* = 10.1 Hz), 5.90 (H-2, *d*,1H, *J* = 10.1 Hz), 2.29 (H-5, *dd*, 1H), 1.28 (H-6, *m*, 1H), 1.39 (H-6, *m*, 1H), 1.27 (H-7, *m*, 1H), 2.06 (H-8, *dd*, 1H), 1.66 (H-11, *m*, 1H), 2.17 (H-11, *m*, 1H), 1.22 (H-15, *m*, 1H), 1.87 (H-16, *m*, 1H), 1.90 (H-17, *m*, 1H), 1.00 (H-18, *s*, 3H), 0.78 (H-19, *d*, 1H), 1.45 (H-19, *d*, 1H), 2.70 (H-20, *m*, 1H), 2.05 (H-22, *m*, 1H), 1.06 (H-28, *s*, 3H), 1.09 (H-29, *s*, 3H), 0.89 (H-30, *s*, 3H)	+	+	+	+	nd	nd	nd

No	Metabolite	Data of NMR (ppm)	Sample in kGy [1)]						
			0	1	5	10	15	20	25
20	Kleinhospitine E	6.79 (H-1, *d*, 1H, *J* = 10.1 Hz), 5.97 (H-2, *d*, 1H, *J* = 10.1 Hz), 2.11 (H-5, *dd*,1H), 1.11 (H-6, *m*,1H), 1.57 (H-6, *m*, 1H), 2.10 (H-8, *t*, 1H), 1.62 (H-11, *m*, 1H), 1.88 (H-11, *m*, 1H), 1.23 (H-12, *m*, 1H), 1.84 (H-12, *m*, 1H), 1.41 (H-15, *m*, 1H), 1.52 (H-15, *m*, 1H), 1.98 (H-16, *m*, 1H), 0.83 (H-18, *s*, 3H), 0.67 (H-19, *d*, 1H, *J* = 5.03 Hz), 1.32 (H-19, *d*, 1H, *J* = 5.03 Hz), 6.64 (H-22, *s*, 1H), 5.65 (H-24, *s*, 1H), 2.28 (H-26, *s*, 3H), 0.96 (H-27, *s*, 3H), 1.09 (H-28, *s*, 3H), 1.01 (H-29, *s*, 3H)	+	+	+	+	+	+	+

[1)]The 0 kGy samples are *K. hospita* samples that were not exposed to GI. 1, 5, 10, 15, 20, and 25 kGy sample refers to a *K. hospita* sample treated to GI at a dose of 1, 5, 10, 15, 20, and 25 kGy. +: metabolites detected in the ^{1}H-NMR spectra of *K. hospita*, nd: metabolites not detected in the ^{1}H-NMR spectra of *K. hospita*. Multiplicity in NMR includes singlet (*s*), doublet (*d*), triplet (*t*), double of doublets (*dd*), and multiplet (m)

Relative Quantification ^{1}H-NMR Analysis

Some metabolites were successfully quantified in all *K. hospita* sample, such as valine, glycine, leucine, phenylalanine, formic acid, malic acid, myo-inositol, adenosine, glucose, sucrose, cycloartan-1,24-diene-3,23-dione, (9*R*,10*R*,23*R*)-21,23;23,27-diepoxycycloartan-1,24-diene-3,27-dione, (9*R*,10*R*,21*S*,23*R*)-21/23,23/27-diepoxy-21-methoxycycloartan-1,24-diene-3,27-dione, and kleinhospitine E by the relative quantification ^{1}H-NMR methods. The results of the quantifications are depicted in Table 2. Nevertheless, the quantification of the remaining metabolites was impeded by their significant signal overlap. The quantified metabolites in the *K. hospita* sample that was treated with GI were compared with those in the untreated *K. hospita* sample.

Quantitative metabolite analysis revealed statistically significant differences in the metabolite profile of *K. hospita* exposed to GI at 10 kGy or higher compared with the control group. Notably, several key metabolites, including amino acids and cycloartane triterpenoids, were detected at lower concentrations. This reduction is consistent with previous research showing a decrease in amino acid content in certain plant species following high-dose GI. The observed changes are primarily due to radiolysis of water within plant cells. This process generates highly reactive free radicals, predominantly •OH. These free radicals readily attack protein molecules and free amino acids, leading to fragmentation, aggregation, or fundamental alterations in their chemical structure [31-32]. A decline in triterpenoid levels has also been reported in various plants subjected to GI. High irradiation doses can directly degrade the chemical bonds within triterpenoids, thereby disrupting their structure. Furthermore, the free radicals generated during GI can induce isomerization or oxidation reactions, which either form new derivatives or result in a net reduction in the original compound level [33].

Table 2. The concentration of metabolites identified in *K. hospita* sample

No	Metabolite	Chemical shift	Concentration[1)]			
			0	1	5	10*
1	Valine	0.85	6.31±0.09	6.55±0.27	6.71±0.05	1.11±0.07
2	Glycine	3.95	6.61±0.08	6.20±0.05	5.44±0.04	nd
3	Leucine	3.36	6.25±0.04	6.43±0.03	6.60±0.03	nd
4	Phenyl alanine	7.40	1.81±0.03	1.81±0.03	1.55±0.02	nd
5	Formic acid	8.41	5.08±0.11	5.08±0.02	3.81±0.05	nd
6	Malic acid	4.28	6.33±0.07	6.40±0.01	4.25±0.07	1.80±0.04
7	Myo-inositol	3.20	1.72±0.04	1.70±0.02	1.68±0.06	0.58±0.05
8	Adenosine	8.21	0.45±0.07	0.54±0.10	0.56±0.07	0.72±0.02
9	Glucose	5.25	6.70±0.09	6.78±0.07	6.91±0.04	7.21±0.06

No	Metabolite	Chemical shift	Concentration[1)]			
			0	1	5	10*
10	Cycloartan-1,24-diene-3,23-dione	2.15	1.72±0.06	1.69±0.05	1.60±0.07	0.36±0.02
11	(9*R*,10*R*,23*R*)-21,23;23,27-diepoxycycloartan-1,24-diene-3,27-dione	2.22	6.77±0.05	6.68±0.04	5.05±0.03	1.35±0.04
12	(9*R*,10*R*,21*S*,23*R*)-21/23,23/27-diepoxy-21-methoxycycloartan-1,24-diene-3,27-dione	1.45	1.63±0.04	1.63±0.03	1.63±0.02	0.36±0.04
13	Kleinhospitine E	2.29	4.62±0.03	4.58±0.06	3.35±0.05	1.13±0.05
	p-value[2)]			0.96	0.58	< 0.05

No	Metabolite	Chemical shift	Concentration[1)]			*p*-value[2)]
			15*	20*	25*	
1	Valine	0.85	nd	nd	nd	<0.05
2	Glycine	3.95	nd	nd	nd	<0.05
3	Leucine	3.36	nd	nd	nd	<0.05
4	Phenyl alanine	7.40	nd	nd	nd	<0.05
5	Formic acid	8.41	nd	nd	nd	<0.05
6	Malic acid	4.28	1.62±0.07	1.26±0.09	0.08±0.03	<0.05
7	Myo-inositol	3.20	nd	nd	nd	<0.05
8	Adenosine	8.21	1.17±0.07	1.22±0.09	1.22±0.08	<0.05
9	Glucose	5.25	7.55±0.06	7.75±0.04	8.01±0.05	<0.05
10	Cycloartan-1,24-diene-3,23 dione	2.15	nd	nd	nd	<0.05
11	(9*R*,10*R*,23*R*)-21,23;23,27-diepoxycycloartan-1,24-diene-3,27-dione	2.22	nd	nd	nd	<0.05
12	(9*R*,10*R*,21*S*,23*R*)-21/23,23/27-diepoxy-21-methoxycycloartan-1,24-diene-3,27-dione	1.45	nd	nd	nd	<0.05
13	Kleinhospitine E	2.29	0.90±0.05	0.81±0.11	0.72±0.08	<0.05
	p-value[2)]		<0.05	<0.05	<0.05	

[1)]The concentration of metabolites in the *K. hospita* sample was expressed as mM. This data represents the average ± the standard deviation (SD). The SD (six repeats) is less than 0.5, indicating that the extraction is reproducible. [2)]The values were derived from one-way ANOVA for each metabolite. *The group indicates statistically significant differences (*p*-value < 0.05) in comparison to the control group

Intriguingly, glucose concentrations were higher in the gamma-irradiated samples than in the non-irradiated control group. This phenomenon is likely attributable to the high energy of gamma irradiation, which can cause the degradation of cell wall components, specifically pectin and hemicellulose within the middle lamella, through the formation of free radicals. The breakdown of the cell wall structure induced by GI leads to an increase in glucose content. Reports by several studies detailing cell wall damage in various plant tissues, including strawberry, orange, and other plants, further support this observation [34]. This evidence suggests that high-dose GI influences the middle lamella, chemically breaking down the structural polysaccharides within the cell wall.

Metabolomic Analysis

A comprehensive examination of the similarities and differences among all samples was conducted by analyzing data derived from the ^{1}H-NMR spectrum, using metabolomic analysis with both unsupervised and supervised multivariate statistical methods. PCA is an unsupervised analytical method used to identify outliers within a dataset and to visualize the inherent clustering tendencies of samples before applying a supervised classification model. In this work, the PCA model captured 69.2% of the total variance, achieving a cross-validated Q^2 of 0.725 and an R^2 of 0.881. The 69.2% variance indicates that the model successfully reduced

the data dimensionality to a few principal components while retaining 69.2% of the unique information or differentiation present in the original dataset. Furthermore, the constructed PCA model effectively explained 88.1% of the data variance and accurately predicted approximately 72.5% of the variance in new data. In multivariate analysis, PCA data are generally considered to have strong confidence in their fit and predictive capacity if the variance captured exceeds 65%, the R^2 value is greater than 0.8, and the Q^2 value is greater than 0.5. Consequently, the clustering pattern derived by the PCA model is highly confident and valid.

As illustrated in the PCA score plot (Fig. 3(a)), low-dose samples (1 and 5 kGy GI) clustered tightly with the untreated control group along the negative axis of PC1. This shows that the metabolite profiles of the 1 and 5 kGy dose groups are very similar to those of the control group. Conversely, on the opposite side (positive PC1 axis), the 20 kGy dose group appeared in close proximity to the 25 kGy group, demonstrating substantial similarity between these two high-dose groups. This clear spatial separation between the high- and low-dose clusters highlights significant differences in metabolite profiles between samples irradiated at low versus high doses. Furthermore, the 15 kGy treatment group occupied a distinct region within the PCA score plot. Although positioned on the positive side of PC1, the 15 kGy group was significantly separated along the negative PC2 axis, suggesting that the 15 kGy dose resulted in a unique metabolic signature compared to all other sample groups.

Further investigation using PLSDA as a supervised model was conducted to analyze the metabolite profiles of all *K. hospita* samples. PLSDA is a supervised analytical method based on partial least squares regression, exhibiting excellent discriminative capability and yielding a classification model for the examined groups. The PLSDA model exhibited total variations of 0.886 (R^2X) and 0.978 (R^2Y). This demonstrates that 88.6% of the variability within the predictor data (X-block) and 97.8% of the variability in the response data (Y-block) were explained by the PLSDA model. Consequently, the classification produced by the PLSDA modeling exhibits high congruence. Furthermore, the constructed PLSDA model yielded a Q^2 value of 0.997, indicating that the resulting sample classification is highly robust and well-validated.

The PLSDA score plot (Fig. 3(b)) visually reinforces the natural clustering tendencies captured by the PCA. Although effective separation was achieved for most treatment classes along the PLSDA 1 and PLSDA 2

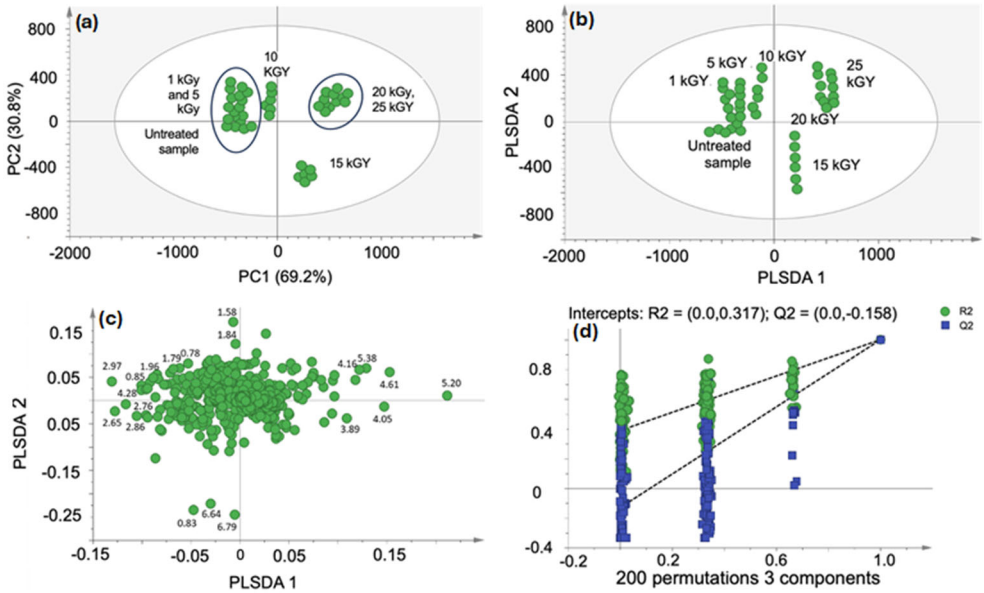

Fig 3. The visualization of the multivariate analysis of the *K. hospita* samples. (a) PCA score plot of *K. hospita*, (b) PLSDA score plot of *K. hospita*, (c) PLSDA loading plot of *K. hospita*, and (d) Permutation test

axes, the untreated control samples remained closely clustered with the low-dose groups (1 and 5 kGy gamma irradiation). This finding indicates that the low-dose treatments did not elicit a metabolic response sufficient to drive a definitive separation from the control. In contrast, the higher-dose groups exhibited apparent dose-specific effects, with the 20 and 25 kGy samples forming a highly similar pair, while the 10 and 15 kGy groups demonstrated robust separation from all other clusters. Analysis of the loading plot (Fig. 3(c)) was employed to identify the compounds that contributed to the differentiation. Metabolites positioned further away from the origin (0,0) exhibit a stronger contribution to the discrimination and explanation of variance observed between the different groups. In the classification of *K. hospita*, valine (buckets at 0.85, 1.96), isoleucine (buckets at 0.78, 1.79, and 4.15), glucose (buckets at 5.20, 4.61), fructose (buckets at 3.89, 4.05), sucrose (buckets at 5.38, 4.16), myo-inositol (bucket at 3.20), malic acid (buckets at 2.65, 4.28), asparagine (bucket at 2.86), aspartic acid (bucket at 2.76), GABA (bucket at 1.87), kleinhospitine E (buckets at 0.83, 6.64, 6.79), and the cycloartan compounds (buckets at 0.79, 0.95, 1.58, 1.84, 2.15, 2.25, 5.89, 5.97, 5.99, 6.33, 6.37, and 6.80) were identified as contributing metabolites based on the loading plot of the first component. To further confirm this PLSDA model, permutation evaluation that is repeated up to 200 times was conducted (Fig. 3(d)). Consequently, the regressions of the Q^2 lines intersecting the y-axis at areas beneath zero [R^2 = (0.0,0.317); Q^2 = (0.0, −0.158)], thereby confirming the model's validity.

Six two-class PLSDA models were developed to enhance the evaluation of distinguishing metabolites for each *K. hospita* sample. The S-plots of these models were analyzed to identify the most significant categories in the differences. The S-Plot demonstrates the strength of the association among intensity (p[1]) and the constancy or reliability (p(corr)1) of a variable in distinguishing chemicals between the two comparison groups. Cutoff criteria of p[1] more than 0.05 and p(corr) more than 0.5 were employed [23]. The S-plot analysis is comprehensively illustrated in Fig. 4.

The model was generated using an untreated sample with treated gamma irradiation doses of 1 kGy (Fig. 4(a)), resulting in R^2X of 75.8%, R^2Y of 99.5%, and Q^2 of 99.0%. The corresponding S-plot analysis revealed that the untreated sample was characterized by malic acid (buckets at 2.65 and 4.28), GABA (bucket at 1.87), valine (buckets at 0.85 and 1.96), and isoleucine (buckets at 1.20 and 4.15). Meanwhile, the *K. hospita* treated with GI at 1 kGy was characterized by glucose (buckets at 5.25 and 3.56) and fructose (buckets at 4.07, 4.13, and 3.88). The model comparing untreated samples with those treated with GI at 5 kGy yielded similar results. The second model (Fig. 4(b)) yields R^2X of 72.3%, R^2Y of 98.5%, and Q^2 of 98.0%. The S-plot analysis indicated that the untreated sample was characterized by isoleucine (buckets at 1.20 and 4.15), malic acid (buckets at 2.65 and 4.28), valine (buckets at 0.85 and 1.96), myo-inositol (bucket at 3.20), and GABA (bucket at 1.87). In the meantime, *K. hospita* subjected to GI at a dose of 5 kGy exhibited glucose buckets at 5.25 and 3.56, and fructose buckets at 4.07, 4.13, and 3.88.

The R^2X, R^2Y, and Q^2 values for the third model, constructed between untreated and gamma-irradiated (10 kGy) samples, were 78.3, 99.2, and 99.0%, respectively. The untreated sample was characterized by (9*R*,10*R*,23*R*)-21,23;23,27-diepoxycycloartan-1,24-diene-3,27-dione (buckets at 2.25, 5.99, 6.35), malic acid (buckets at 2.65, 4.28), and GABA (bucket at 1.87). The corresponding S-plot analysis confirmed these findings (Fig. 4(c)). Furthermore, the *K. hospita* that were exposed to GI with dosages of 10 kGy were characterized by glucose (buckets at 5.25 and 3.56), fructose (buckets at 4.07, 4.13, and 3.88), and adenosine (buckets at 8.17).

In the following model (Fig. 4(d)), which included both untreated and 15 kGy gamma-irradiated samples, the R^2X, R^2Y, and Q^2 values were 80.5, 99.6, and 99.0%, respectively. Kleinhospitine E (buckets at 6.79, 5.97, 0.83, 1.32, 6.64), (9*R*,10*R*,23*R*)-21,23;23,27-diepoxycycloartan-1,24-diene-3,27-dione (buckets at 2.25, 5.99, 6.35), malic acid (buckets at 2.65, 4.28), and GABA (bucket at 1.87) were the characterizations of the untreated sample. These results were confirmed by the S-plot analysis that accompanied them. Additionally, glucose (buckets at 5.25 and 3.56), fructose (buckets at 4.07, 4.13, and 3.88), and adenosine (bucket at 8.17) were

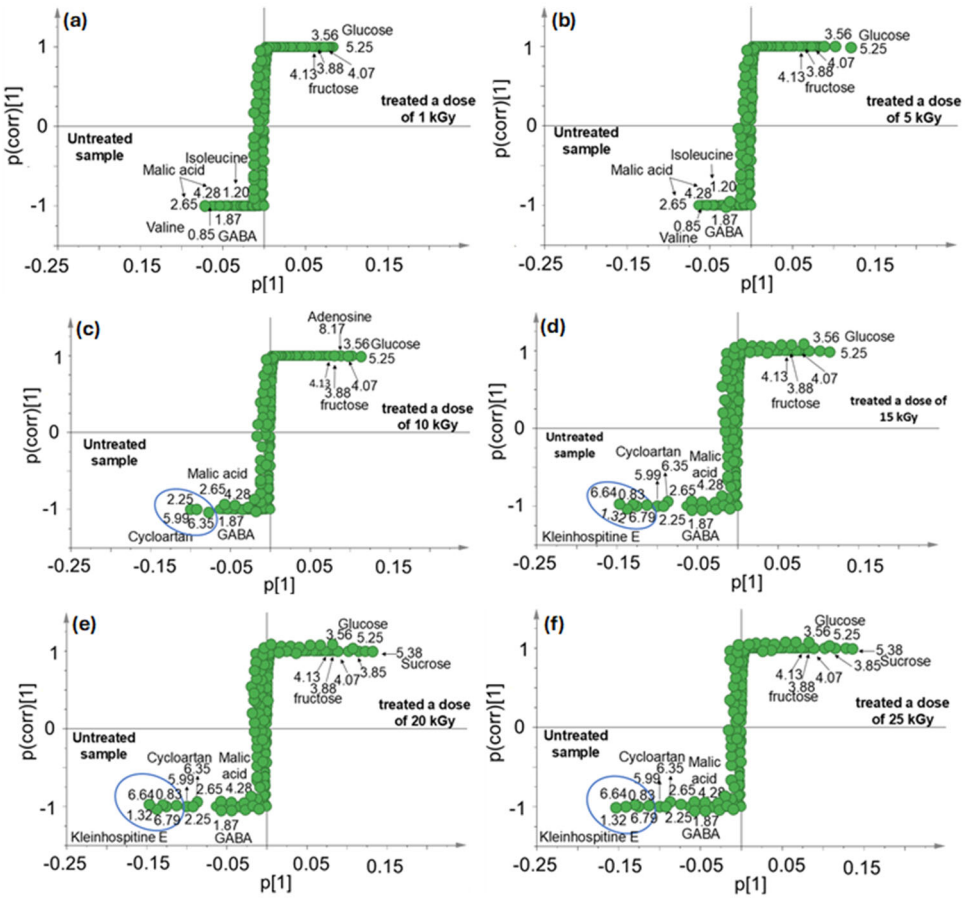

Fig 4. S-plot developed from the six two-class PLSDA approaches. (a) Untreated and treated GI doses 1 kGy groups, (b) untreated and treated GI doses 5 kGy groups, (c) Untreated and treated GI doses 10 kGy groups, (d) Untreated and treated GI doses 15 kGy groups, (e) Untreated and treated GI doses 20 kGy groups, (f) Untreated and treated GI doses 25 kGy groups

described in *K. hospita* treated with GI at 15 kGy. Similar results were observed in the fifth (Fig. 4(e)) and sixth (Fig. 4(f)) models, which were constructed by comparing the untreated control group with the groups exposed to 20 and 25 kGy of GI, respectively. The statistical parameters for each model consistently demonstrated that the two-class PLS-DA models were robust and valid. Specifically, the models exhibited R^2X values exceeding 71.5%, R^2Y values exceeding 98.4%, and predictive Q^2 values exceeding 93.8%.

Subsequently, the variable Importance in projection (VIP) scores were calculated to rank the metabolites that contributed the most to the variance between the non-irradiated and GI groups. Variables with a VIP score greater than 1 were deemed important discriminators for the model. The resulting VIP values for the identified *K. hospita* metabolites are presented in Table 3. The data in Table 3 indicate the presence of several metabolites that are critical for distinguishing between the gamma-irradiated and non-irradiated control groups. These compounds include the amino acids valine, glycine, isoleucine, leucine, asparagine, and aspartic acid, along with the carbohydrates glucose, fructose, and sucrose, and the cycloartane triterpenoid (9*R*,10*R*,21*S*,23*R*)-21/23,23/27-diepoxy-21-methoxycycloartan-1,24-diene-3,27-dione. Specifically, amino acids, particularly valine, exhibited the highest VIP score of 1.61. This outcome indicates that amino acids are the most critical class of metabolites for distinguishing the untreated control group from the GI groups. The PLSDA score plot

Table 3. A tabular representation of VIP values for identified *K. hospita* metabolites

No	Metabolite	Chemical shift	VIP score
1	Valine	0.85	1.61
		1.96	1.52
2	Glycine	3.95	1.44
3	Isoleucine	0.78	1.34
		1.79	1.38
		4.15	1.13
4	Leucine	1.20	1.24
		1.79	1.20
5	Asparagine	2.86	1.40
6	Aspartic acid	2.76	1.05
7	Phenylalanine	7.28	0.85
8	Formic acid	8.41	0.66
9	Malic acid	2.65	0.98
		4.28	0.96
10	GABA	1.87	0.64
11	Myo-inositol	3.20	0.52
12	Adenosine	8.21	0.66
13	Glucose	5.20	1.23
		4.61	1.19
14	Fructose	3.89	1.05
		4.05	1.07
15	Sucrose	5.38	1.15
		4.16	1.12
16	Cycloartan-1,24-diene-3,23 dione	6.37	0.56
		5.89	0.51
17	(9*S*,10*S*,21*R*,23*S*)-2½3,23/27-diepoxy-21-methoxycycloartan-1,24-diene-3,27-dione	6.77	0.54
		0.95	0.53
18	(9*R*,10*R*,23*R*)-21,23;23,27-diepoxycycloartan-1,24-diene-3,27-dione	6.33	0.99
		5.96	1.01
19	(9*R*,10*R*,21*S*,23*R*)-2½3,23/27-diepoxy-21-methoxycycloartan-1,24-diene-3,27-dione	6.38	0.52
		5.90	0.77
20	Kleinhospitine E	0.83	0.72
		6.64	0.73
		6.79	0.66

further elucidated this finding, revealing that valine (represented by buckets at 0.85) was positioned in the negative region of the first PLSDA component (PLSDA 1 negative). This position is opposed to the region occupied by the 20 and 25 kGy treatment groups. This spatial arrangement indicates a substantial difference in valine abundance between the non-irradiated and low-dose groups (1 and 5 kGy) and the high-dose groups (20 and 25 kGy). This result is further corroborated by metabolite quantification data, which showed a consistent decline in amino acid levels, including valine, concomitant with increasing irradiation dose.

Another class of metabolites observed to be critical in differentiating the tested groups was cycloartane triterpenoids. This finding is consistent with both the PLSDA model and the metabolite quantification data, which revealed a significant reduction in these compounds following GI at doses above 10 kGy. The

identified decrease in both amino acids and triterpenoids is primarily attributable to GI's indirect effect: the formation of free radicals. These radicals are capable of attacking chemical bonds in the amino acid side chains, leading to deamination and decarboxylation, as well as causing the cleavage of double bonds inherent to the triterpenoid structures [33-35]. The resulting decline in amino acid and cycloartane triterpenoid concentrations within *K. hospita* samples can negatively impact both the plant's cellular integrity and its bioactive potential. Specifically, cycloartane triterpenoids have been reported as key compounds responsible for anti-inflammatory and anticancer activities [4].

Furthermore, sucrose, glucose, and fructose were also identified as discriminating metabolites among the tested groups. The PLSDA score plot revealed that these carbohydrates were positioned in the positive region of the first component (PLSDA 1 positive), which is opposed to the control group and the low-dose GI groups. This spatial arrangement indicates that higher GI doses (up to 25 kGy) are associated with higher sugar concentrations in *K. hospita* samples. The observed concurrent shifts in the metabolite profiles of amino acids, cycloartane triterpenoids, and sugars collectively indicate that GI significantly alters the metabolome of *K. hospita*. Consequently, careful consideration of the applied gamma irradiation dose is crucial for product quality and the biological activity of *K. hospita*.

■ CONCLUSION

In conclusion, the results presented above demonstrate that the metabolites in *K. hospita* can be influenced by GI. The degree of the alteration is contingent upon the dosage that was given. When *K. hospita* was subjected to GI at 10 kGy, the sugar content of the sample increased, and the characteristic signs of cycloartan triterpenoids disappeared. The sample shows a greater increase in sugar and a decline in the characteristic signals of these triterpenoids as the GI dose increases. Conversely, there was no statistically significant difference in metabolites at modest doses (1–5 kGy). This finding suggests that it has the potential to reduce the risk of contaminants without significantly altering the sample's metabolite profile at dosages below 10 kGy.

■ ACKNOWLEDGMENTS

This research was funded by the Ministry of Education, Culture, Research, and Technology through a fundamental research grant, as detailed in Agreement Letter number 612/UN/17.L1/HK/2024. We are deeply appreciative of the Merah Putih Gamma Irradiator (IGMP) for its gamma irradiation facilities and to DJ Botanicals for providing *K. hospita* samples and facilities.

■ CONFLICT OF INTEREST

The authors declare that there are no conflicts of interest related to the publication of this article.

■ AUTHOR CONTRIBUTIONS

Islamudin Ahmad, Lizma Febrina, Baso Didik Hikmawan: conceptualize, design the work, and draft manuscripts; Amal Rezka Putra, Arman Rusman, Arsyik Ibrahim, Supriatno Salam: Gamma irradiation treatment and data analysis for analysis; Erwin Samsul, Hidzfur Rashif Rija'i, Muhammad Arifudin, Iswahyudi: preparation of sample and drafting manuscripts; Ratna Surya Alwi, Gemini Alam, Abdul Mun'in: interpretation of data and finalization of manuscripts.

■ REFERENCES

[1] Damayanti, S., Fabelle, N.R., Yooin, W., Insanu, M., Jiranusornkul, S., and Wongrattanakamon, P., 2021, Molecular modeling for potential cathepsin L inhibitor identification as new anti-photoaging agents from tropical medicinal plants, *J. Bioenerg. Biomembr.*, 53 (3), 259–274

[2] Frankova, A., Vistejnova, L., Merinas-Amo, T., Leheckova, Z., Doskocil, I., Wong Soon, J., Kudera, T., Laupua, F., Alonso-Moraga, A., and Kokoska, L., 2021, *In vitro* antibacterial activity of extracts from Samoan medicinal plants and their effect on proliferation and migration of human fibroblasts, *J. Ethnopharmacol.*, 264, 113220.

[3] Ariefta, N.R., Sofian, F.F., Aboshi, T., Kuncoro, H., Dinata, D.I., Shiono, Y., and Nishikaw, Y., 2024, Evaluation of the antiplasmodial and anti-*Toxoplasma* activities of several Indonesian

medicinal plant extracts, *J. Ethnopharmacol.*, 331, 118269

[4] Rahim, A., Saito, Y., Miyake, K., Goto, M., Chen, C.H., Alam, G., Morris-Natschke, S., Lee, K.H., and Nakagawa-Goto, K., 2018, Kleinhospitine E and cycloartane triterpenoids from *Kleinhovia hospita*, *J. Nat. Prod.*, 81 (7), 1619–1627.

[5] Alani, F.W., Djabir, Y.Y., and Arsyad, M.A., 2023, *Kleinhovia hospita* leaf extract protects the heart against infarction by isoproterenol, *Iran. J. Toxicol.*, 17 (2), 87–94.

[6] Tayeb, R., Alam, G., Pakki, E., and Djabir, Y.Y., 2019, Paliasa (*Kleinhovia hospita* L.) hepatoprotector 'tea bag' preparation as supporting therapy in the use of fixed-dose combination of antituberculosis drugs, *J. Phys.: Conf. Ser.*, 1341 (7), 072016.

[7] Opuni, K.F.M., Kretchy, J.P., Agyabeng, K., Boadu, J.A., Adanu, T., Ankamah, S., Appiah, A., Amoah, G.B., Baidoo, M., and Kretchy, I.A., 2023, Contamination of herbal medicinal products in low-and-middle-income countries: A systematic review, *Heliyon*, 9 (9), e19370.

[8] Casu, A., Camardo Leggieri, M., Toscano, P., and Battilani, P., 2024, Changing climate, shifting mycotoxins: A comprehensive review of climate change impact on mycotoxin contamination, *Compr. Rev. Food Sci. Food Saf.*, 23 (2), e13323.

[9] Molnár, K., Rácz, C., Dövényi-Nagy, T., Bakó, K., Pusztahelyi, T., Kovács, S., Adácsi, C., Pócsi, I., and Dobos, A., 2023, The effect of environmental factors on mould counts and AFB1 toxin production by *Aspergillus flavus* in maize, *Toxins*, 15 (3), 227.

[10] Ansari, F.A., Perazzolli, M., Husain, F.M., Khan, A.S., Ahmed, N.Z., and Meena, R.P., 2024, Novel decontamination approaches for stability and shelf-life improvement of herbal drugs: A concise review, *Microbe*, 3, 100070.

[11] Rahmati, E., Khoshtaghaza, M., Banakar, A., and Ebadi, M.T., 2022, Decontamination technologies for medicinal and aromatic plants: A review, *Food Sci. Nutr.*, 10 (3), 784–799.

[12] Schottroff, F., Lasarus, T., Stupak, M., Hajslova, J., Fauster, T., and Jäger, H., 2021, Decontamination of herbs and spices by gamma irradiation and low-energy electron beam treatments and influence on product characteristics upon storage, *J. Radiat. Res. Appl. Sci.*, 14 (1), 380–395.

[13] Hadiati, S.W., Winarno, H., and Pramono, S., 2021, Gamma irradiation as suitable preservation method on herbal medicine, *Food Res.*, 5 (5), 33–42.

[14] Riviello-Flores, M.L., Cadena-Iñiguez, J., Ruiz-Posadas, L.D., Arévalo-Galarza, M.D., Castillo-Juárez, I., Soto Hernández, M., and Castillo-Martínez, C.R., 2022, Use of gamma radiation for the genetic improvement of underutilized plant varieties, *Plants*, 11 (9), 1161.

[15] Komara, I., Susanto, A., Amaliya, A., Abbas, B., Warastuti, Y., Hendiani, I., Mirada, A., and Erliani, A.P., 2023, The effect of gamma-ray irradiation on the physical, mechanical, and morphological characteristics of PVA-collagen-chitosan as a guided tissue regeneration (GTR) membrane material, *Eur. J. Dent.*, 17 (2), 530–538.

[16] Aleksieva, K., Mladenova, R., Taneva, S., Denev, P., and Karakirova, Y., 2025, Effect of gamma irradiation on free radicals and the antioxidant properties of walnuts, *Chemistry*, 7 (2), 52.

[17] Aleksieva, K.I., Mladenova, R.B., Solakov, N.Y., Loginovska, K.K., and Dimov, K.G., 2025, Gamma radiation effects on free radicals, antioxidant activity, phenolic and flavonoid content in royal jelly, *Radiat. Phys. Chem.*, 226, 112231.

[18] Galeaz, C., Totis, C., and Bisio, A., 2021, Radiation resistance: A matter of transcription factors, *Front. Oncol.*, 11, 662840.

[19] Katiyar, P., Pandey, N., and Keshavkant, S., 2022, Gamma radiation: A potential tool for abiotic stress mitigation and management of agroecosystem, *Plant Stress*, 5, 100089.

[20] Choi, H.I., Han, S.M., Jo, Y.D., Hong, M.J., Kim, S.H., and Kim, J.B., 2021, Effects of acute and chronic gamma irradiation on the cell biology and physiology of rice plants, *Plants*, 10 (3), 439.

[21] Ahmad, I., Febrina, L., Hikmawan, B.D., Junaidin, J., Herman, H., Faisal, M., Samsul, E., Iswahyudi, I., Ibrahim, A., Purwoko, R.Y., Okselni, T., Angelina,

M., Putra, A.R., Alwi, R.S., and Mun'im, A., 2024, NMR-based metabolic profiling and antioxidant activity of *Eleutherine bulbosa* bulb ethanol extract, *Nat. Prod. Res.*, 39 (24), 7096–7103.

[22] Netrprachit, P., Nuangchamnong, N., Ramli, N.S., Maulidiani, M., Mediani, A., Zolkeflee, N.K.Z., Jiamyangyuen, S., and Abas, F., 2023, Bioactive compounds of pigmented rice extracts reveal by NMR-based metabolomics, *CyTA – J. Food*, 21 (1), 760–770.

[23] Febrina, L., Happyana, N., and Syah, Y.M., 2023, Metabolic profiling, antioxidant activity, and alpha-glucosidase inhibitory activity of the roasted beans of luwak (civet) coffee, *ACS Food Sci. Technol.*, 3 (11), 1864–1876.

[24] Satmoko, A., Gunawan, H.A., Kardos, R., Rozali, B., and Purwadi, M.D., 2020, Commissioning test of the iradiator gamma merah putih, *J. Phys.: Conf. Ser.*, 1436 (1), 012017.

[25] Gao, X., Niu, J., Xiao, Z., Rong, D., Yu, M., Sy, B., Wang, C., and Lv, Z., 2025, The application of quantitative ^{1}H-NMR for the determination of melatonin and vitamin B6 in commercial melatonin products, *Molecules*, 30 (14), 2942.

[26] Dona A.C., Kyriakides, M., Scott, F., Shephard, E.A., Varshavi, D., Veselkov, K., and Everett, J.R., 2016, A guide to the identification of metabolites in NMR-based metabonomics/metabolomics experiments, *Comput. Struct. Biotechnol. J.*, 14, 135–153.

[27] Alexandersson, E., and Nestor, G., 2022, Complete ^{1}H and ^{13}C spectral assignment of D-glucofuranose, *Carbohydr. Res.*, 511, 108477.

[28] Febrina, L., Happyana, N., and Syah, Y.M., 2022, Identifying metabolites in complex extract of sigararutang coffee beans with NMR spectroscopy method, *Moroccan J. Chem.*, 10 (2), 298–307.

[29] Devi, K., and Awasthi, P., 2022, Isoleucine with secondary sulfonamide functionality as anticancer, antibacterial and antifungal agents, *J. Biomol. Struct. Dyn.*, 40 (15), 7052–7069.

[30] Chaloupecká, E., Tyrpekl, V., Bártová, K., Nishiyama, Y., and Dračínský, M., 2024, NMR crystallography of amino acids, *Solid State Nucl. Magn. Reson.*, 130, 101921.

[31] Asmarani, R.R., Ujilestari, T., Solikin, M.M., Wulandari, W., Damayanti, E., Anwar, M., Aditya, S., Karimy, M.F., Wahono, S.K., Triyannanto, E., Adli, D.N., Surjawanta, S.O., and Wahyono, T., 2024, Meta-analysis of the effects of gamma irradiation on chicken meat and meat product quality, *Vet World*, 17 (5), 1084–1097.

[32] Hota, S., Shams, R., Dash, K.K., Pawase, P.A., Mukarram, S.A., and Kovács, B., 2025, A comprehensive review on the potential role of irradiation technique on techno-functional properties of plant-based proteins, *J. Agric. Food Res.*, 23, 102095.

[33] da Silva, M.M., Diniz, E.C., Maia Neto, L.S., Araujo, L.A., Magnata, S.S.L.P., de Jesus Amaral, A., Maciel Netto, A., and da Silva, E.B., 2025, Analysis of the relationship between absorbed dose and its effect on plant materials: A literature review, *Braz. J. Radiat. Sci*, 13 (3A), 1–24.

[34] Li, X., Wang, B., Hu, W., Chen, H., Sheng, Z., Yang, B., and Yu, L., 2022, Effect of γ-irradiation on structure, physicochemical property and bioactivity of soluble dietary fiber in navel orange peel, *Food Chem.: X*, 14, 100274.

[35] Majumdar, C.G., ElSohly, M.A., Ibrahim, E.A., Elhendawy, M.A., Stanford, D., Chandra, S., Wanas, A.S., and Radwan, M.M., 2023, Effect of gamma irradiation on cannabinoid, terpene, and moisture content of cannabis biomass, *Molecules*, 28 (23), 7710.